Green Chemistry

PAPER

View Article Online
View Journal

Cite this: DOI: 10.1039/d4gc01961j

Thymol: nature's solvent for sustainable hollow fiber fabrication†

Usman T. Syed,‡[a] Lakshmeesha Upadhyaya, ‡[a] Livia M. D. Loiola,[a] Abdul-Hamid Emwas,[b] Alexey Volkov[a] and Suzana P. Nunes *[a,c]

Received 20th April 2024,
Accepted 30th July 2024

DOI: 10.1039/d4gc01961j

rsc.li/greenchem

Sustainable separation processes are crucial for industries like chemicals and pharmaceuticals and membrane technology stands out for its low energy consumption. However, membrane fabrication typically involves large amounts of solvents, which are facing tighter scrutiny due to environmental regulations. This work tackles the quest to replace toxic solvents and proposes thymol and its mixtures with other natural components as green solvents. Thymol, despite being solid at room temperature, forms homogeneous liquid solutions with a high-performance polyetherimide, exhibiting behavior analogous to deep eutectic mixtures observed for small molecules. Through spectroscopic, thermal, and rheological analyses, we elucidate the role of hydrogen bonding between carbonyl and hydroxyl groups in these solutions. We utilized the findings for membrane fabrication. Hollow fibers were spun in continuous machines using the green solvent dope solutions. These fibers coated with polyphenols were assessed for air dehumidification, showcasing the successful translation of fundamental investigation into membrane production and application.

Introduction

The chemical industry must be more sustainable, minimizing the negative environmental and health impacts of its processes and product manufacturing, preventing toxic discharge and the exposure of staff and final users to concerning substances. This is expected to happen while keeping or enhancing economic competitiveness. The need for changes drives opportunities and the search for sustainable solutions might enable new technologies and access to products not available today. However, fulfilling all requirements for sustainability is highly challenging. To propel the implementation of several sustainability goals, Europe has been a pioneer in regulations for the use of chemicals, which eventually gets adopted in other parts of the world. The Registration, Evaluation, Authorization and Restriction of Chemicals regulations by the European Chemicals Agency protect human health and the environment by identifying hazardous chemicals. These restrictions are percolating to all chemical-based manufacturing sectors. The fabrication of membranes for water, biomedical, food and chemical separations is heavily based on organic solvents, such as *N*,*N*-dimethylformamide (DMF) or *N*-methyl-2-pyrrolidone (NMP). Due to increasing concerns about the carcinogenic, toxic to reproduction, and respiratory sensitizing effects of DMF,[1] the European Union has recently raised restrictions on its use requiring stricter risk management and operational condition control.[2] NMP has been marked to be used only if strict exposure limits are ensured. The industry must be prepared to substitute their processes and use more sustainable solvents in the future.[3,4] Additionally, in the last few years, the United States Environmental Protection Agency and the Occupational Safety and Health Administration agency are spearheading to impose a ban on toxic substances.[5,6]

This work tackles the quest for finding alternative sustainable solvents for polymers with particular interest for the fabrication of membranes for sustainable separations. Synthetic membranes are produced as flat sheets and hollow fibers. Their complex morphology, essential for membrane performance, is highly influenced by the thermodynamics of polymer–solvent interactions and by the kinetics of phase separation processes induced during the fabrication process by exposure to a non-solvent. Therefore, the challenge is not only the polymer solubilization, but also the full control of thermodynamic and rheological aspects leading to the required pore

[a]*Environmental Science and Engineering Program, Biological and Environmental Science and Engineering Division (BESE), King Abdullah University of Science and Technology (KAUST), 23955-6900 Thuwal, Saudi Arabia.*
E-mail: suzana.nunes at kaust.edu.sa
[b]*Core Labs, King Abdullah University of Science and Technology (KAUST), 23955-6900 Thuwal, Saudi Arabia*
[c]*Chemistry Program and Chemical Engineering Program, Physical Science and Engineering Division (PSE), King Abdullah University of Science and Technology (KAUST), 23955-6900 Thuwal, Saudi Arabia*

†Electronic supplementary information (ESI) available. See DOI: https://doi.org/10.1039/d4gc01961j

‡Equal contributions as first author.

structure morphology when a traditional solvent is substituted by an alternative.

The best solutions come from nature. Hydrogen bonds are essential for functions and processes in living organisms, driving the formation of biological structures, recognition, and association of biomolecules like proteins. Hydrogen bonds are formed by the donation of electron-deficient hydrogen atoms to lone electron pair-containing groups as Lewis acids and bases. Carbonyl and hydroxyl groups are major hydrogen bond acceptors. Hydrogen bonds are strongly connected to the solubilization of highly concentrated substances in plants, which in many times exceed the expected solubility levels in water under comparable thermodynamic conditions of temperature and pressure.[7] Examples are honey and maple syrup, which have low water content.[8] In several examples, natural liquid systems have a significantly lower solid–liquid phase transition temperature compared to those of the single components, justifying their classification as deep eutectic solvents (DESs). They are fundamental to maintain important metabolic functions even in extreme conditions of drought, high salinity, and low temperature. They have been linked to the preservation of enzyme conformations, preventing denaturation, enabling the retention of water and tuning the viscosity for the mobility and transport of biomolecules like nucleic acids.[9]

The solubility of proteins, polysaccharides and phenolic metabolites has been demonstrated to be higher in DESs than in water, stimulating expectations for their potential as green solvents for extraction of bioactive compounds and other applications.[10] We have been inspired by the observations in natural biological systems in the search for new green solvents for polymer membrane fabrication. Many of the mixtures classified as DESs are purely natural with advantages of low vapor pressure, low flammability, high bio-based content, biocompatibility, and low cost.[11–15] Previous research using DESs for polymer systems could be exemplified by five different approaches. The most explored is the use of hydrophilic DESs to dissolve hydrophilic polymers such as cellulose and enable chemical modifications such as conversion into carbamate fibers.[16] Another approach involves the synthesis of polymeric materials, formed by a strong interaction between hydrogen bond donors like polyphenols and an ionic hydrogen bond acceptor (*e.g.*, ammonium).[17] The next two examples explore the self-polymerization ability of monomers (as gelators) without any initiators, forming analogues of iongels termed 'eutectogels',[18,19] and the *in situ* polymerization of DES components to form conducting materials.[20,21] A final example is a block copolymerization conducted in DES medium as a solvent and induced self-assembly.[22]

Our motivation in this work is the full substitution of chemicals like DMF and NMP by natural compounds, providing a sustainable process for membrane fabrication. Almost all previous attempts to use DESs for this purpose have focused on hydrophilic mixtures as additives, pore-forming agents, and co-solvents.[23–25] Ismail *et al.*[25] synthesized *N*-methylacetamide-based hydrophilic DESs with the aim of solubilizing poly(vinylidene fluoride) (PVDF) to produce PVDF membranes, adding polyvinylpyrrolidone (PVP) as a pore-forming agent. We recently used a hydrophilic DES constituted by a mixture of urea and propionic acid to dissolve lignin for membrane preparation.[26] The solubilization of other polymers by hydrophilic DESs has been so far restricted to low concentrations insufficient for membrane casting. Mixtures of hydrophobic natural components with deep eutectic properties have been more recently identified and evaluated for applications mainly centered around (micro) extraction, therapeutics, chemical and environmental purposes.[27–31] Their consideration for membrane related purposes has been restricted as additives or as extractive pore-filling compounds in liquid membranes.[32]

Herein, we innovate first by exploring green solvents for high-performance polymers and for membrane fabrication fully based on hydrophobic natural components that are solid at room temperature. We focus on a series of natural hydrophobic mixtures containing thymol along with aroma compounds.[33] We demonstrate and compare the selected solvent mixtures applied to Ultem®, a polyetherimide whose industrial solvents have been DMF and NMP. Secondly, we contribute to the fundamental understanding of the interactions between the solid compounds and with the polymer through comprehensive chemical characterization employing Nuclear Magnetic Resonance (NMR) and other methods. Our investigation leads to the first report of a binary liquid solution in which one component is a polymer and the other is a single hydrophobic natural solvent, both solid at room temperature. We use the polymer solutions to fabricate hollow fibers, which were scaled up using a dry–jet wet spinning unit, dip-coated with a natural polyphenol layer and tested for air dehumidification.

Results and discussion

Thymol-based solvents for Ultem®

We explored a series of natural compounds and their mixture for the solubilization of Ultem®. The mixtures were constituted by thymol and as a secondary component DL-menthol, raspberry ketone (4-(4-hydroxyphenyl)-2-butanone), and D-camphor at various molar compositions (1 : 1, 4 : 1 and 1 : 4) prepared and stored at 25 °C. All single components are solid at room temperature. The melting temperature of thymol is 49–50 °C. The physicochemical properties of the mixture components are detailed in Table S1.† The glass transition temperature of Ultem® is 207 °C. We initially targeted a dope solution concentration of at least 13 wt% polymer with viscosity adequate for hollow fiber fabrication. As shown in Table S2 and Fig. S1,† all mixtures with a high thymol ratio were able to dissolve the polymer at 70 °C, as well as thymol as a single solvent. As the temperature decreased to 25 °C, only solutions in thymol/raspberry ketone (4 : 1) and pure thymol did not demix. The dope solutions containing DL-menthol and camphor became unstable below 50 °C and 70 °C, respectively. Thus, we selected the mixture 4 : 1 thymol/raspberry ketone which could be used to prepare dope solutions for convenient

hollow fiber spinning close to room temperature. We also observed that pure thymol can conveniently dissolve Ultem®, forming a stable dope solution at room temperature.

The thymol/raspberry ketone solutions were investigated by differential scanning calorimetry (DSC) and NMR spectroscopy to understand the reasons for their behavior as deep eutectic solvents. Hydrogen bonding is expected to play a key role. Fig. 1 shows the characterization of the pure components and their mixtures. Well-defined melting and crystallization peaks for the single components are shown in Fig. 1a, but no peak is seen for the mixture in the investigated range between −70 and 100 °C. It reflects the fact that the mixture is liquid in this temperature range. The molecular arrangement of thymol and raspberry ketone is disrupted in the mixture with the formation of hydrogen bonds between the two components without the possibility of regular packing required for crystallization. The result is the absence of the melting peaks in the DSC curves.

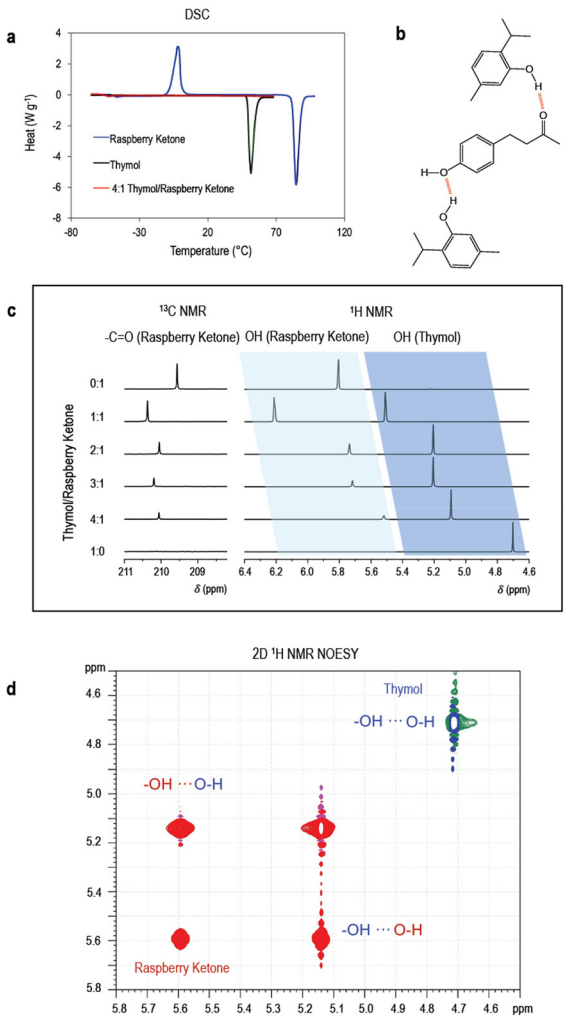

Fig. 1 Thermal and spectroscopic characterization of thymol/raspberry ketone mixtures. (a) Differential scanning calorimetry (DSC) of single components and a 4 : 1 mixture ratio. (b) Diagram depicting hydrogen bond formation. (c) ^{1}H NMR and ^{13}C NMR spectra of mixtures with different thymol/raspberry ketone ratios as evidence of chemical shifts of the carbonyl and hydroxyl ketone peaks and the hydroxyl peak of thymol. (d) 2D ^{1}H NMR NOESY overlap spectra of thymol and a 4 : 1 thymol/raspberry ketone mixture.

NMR spectroscopy elucidates the intermolecular interactions between the mixtures of thymol and raspberry ketone. ^{1}H NMR spectroscopy (Fig. 1c) demonstrates shifts of peaks relative to the hydroxyl groups of thymol and raspberry ketone when mixed in different ratios. ^{1}H NMR chemical shifts (δ_s) are closely related to the molecular electronic structure and intermolecular hydrogen bonding will result in a decrease in the diamagnetic shielding around the hydrogen nucleus. It leads to the resonance of the proton concerned to be shifted to low field. This is referred to as the deshielding effect on the bridging hydrogen atom and ^{1}H δ_s can be used for identifying and characterizing hydrogen bonding.[34] In general, a conventional hydrogen bonding will lead to a chemical shift of the bridging proton to move downfield by 1–4 ppm.

The hydrogen bond interactions between the hydroxyl groups of the two compounds also lead to shifts in the 2D ^{1}H NMR NOESY (Nuclear Overhauser Effect Spectroscopy) spectra (Fig. 1d). NOESY is a proton–proton through space correlation spectroscopy technique, where the transfer of magnetization among the spins can be detected through dipolar coupling. The NOESY spectrum presents diagonal and cross peaks, and the latter represent the nuclei that are close in space rather than coupled with each other *via* covalent bonds.

^{1}H and ^{13}C NMR spectra in $CDCl_3$ for the components are individually shown in Fig. S2–S5.† The spectra of thymol/raspberry ketone mixtures are shown in Fig. S6 and S7.† The difference in chemical shifts ($\Delta\delta$) between thymol and raspberry ketone signals in individual solutions in $CDCl_3$, and their signals in the mixtures diluted in $CDCl_3$, are shown in Table S3.† When hydrogen atoms are drawn by electron-withdrawing elements or groups to form hydrogen bonds, they exhibit downfield chemical shift variations. As depicted in the Fig. 1c and Table S3† for spectra of mixtures with thymol/raspberry ketone with different molar ratios, a downfield shift of the proton peak relative to the thymol OH group occurs as the concentration of raspberry ketone increases. These results indicate the formation of hydrogen bonding, and the interaction scheme is proposed in Fig. 1b, with thymol being a hydrogen bonding donor. The proton signals relative to the raspberry ketone –OH follow a mixed behavior. When comparing raspberry ketone and the 1 : 1 mixture, a downfield shift is seen, indicating that the raspberry ketone hydroxyl oxygen is acting as an H-bond donor. However, as the ratio of thymol increases, the shift inverts to upfield indicating that the oxygen acts as an acceptor as the amount of thymol becomes preponderant. The strongest interaction happens between the proton of the thymol hydroxyl group and the carbonyl group of raspberry ketone, which can be detected by ^{13}C NMR spectroscopy (Fig. 1c and Fig. S7†). The peak shifts from 209.57 ppm to a maximum of 210.37 ppm in the presence of thymol.

The quantification of H-bond accepting or donating ability can be evaluated using ^{31}P NMR spectroscopy, following a procedure reported by Franz and co-workers.[35,36] We used a triethyl phosphine oxide probe in a solution together with

thymol, raspberry ketone or Ultem®. The results are shown in Fig. S8.† Raspberry ketone binding to the probe resulted in the largest shift downfield $\Delta\delta$ (^{31}P) value ($\Delta\delta$ = 4.95 ppm) upon binding to the probe. The $\Delta\delta(^{31}P)$ value for thymol was $\Delta\delta$ = 3.89 ppm. This indicates that raspberry ketone has a higher H-bond donating ability than thymol, if we consider only the –OH group. This can be explained by comparing these two phenolic compounds regarding their electron-withdrawing or donating groups in *ortho*-, *meta*- and *para*-positions. Thymol has *ortho*-isopropyl and *meta*-methyl weak electron-donating groups, while raspberry ketone has a *para*-aliphatic ketone weak electron-withdrawing group. It is reported that within a phenol series, electron-withdrawing groups result in greater $\Delta\delta(^{31}P)$ values upon TEPO binding than electron-donating groups, as observed here. The H-bond donating ability of raspberry ketone explains the downfield shift observed for the 1 : 1 thymol/raspberry ketone mixture (Fig. 1c). However, the carbonyl group of raspberry ketone makes it a strong proton acceptor.

In contrast to thymol and raspberry ketone, Ultem® shifts the phosphine oxide probe ^{31}P peak upfield. No hydroxyl group is available in this case and it itself is a proton acceptor, as discussed later and the carbonyl groups are expected to act similarly to the carbonyl in raspberry ketone. We confirmed that the 4 : 1 thymol/raspberry ketone mixture was able to dissolve Ultem®, and observed that, when heated above its melting temperature, thymol alone could act as a solvent for Ultem®. In both cases, when the temperature is dropped to 25 °C, the solutions remain stable.

Physical characterization of Ultem® dope solutions

Fig. 2 illustrates the solubilization of Ultem® in thymol along with the thermal and rheological properties of these polymeric dope solutions, compared to classical organic solvents like NMP and DMF. Fig. 2b shows the DSC profile of different solutions. Thymol's strong melting peak is visible at 50 °C. For Ultem® solutions in pure thymol, the thymol melting tempera-

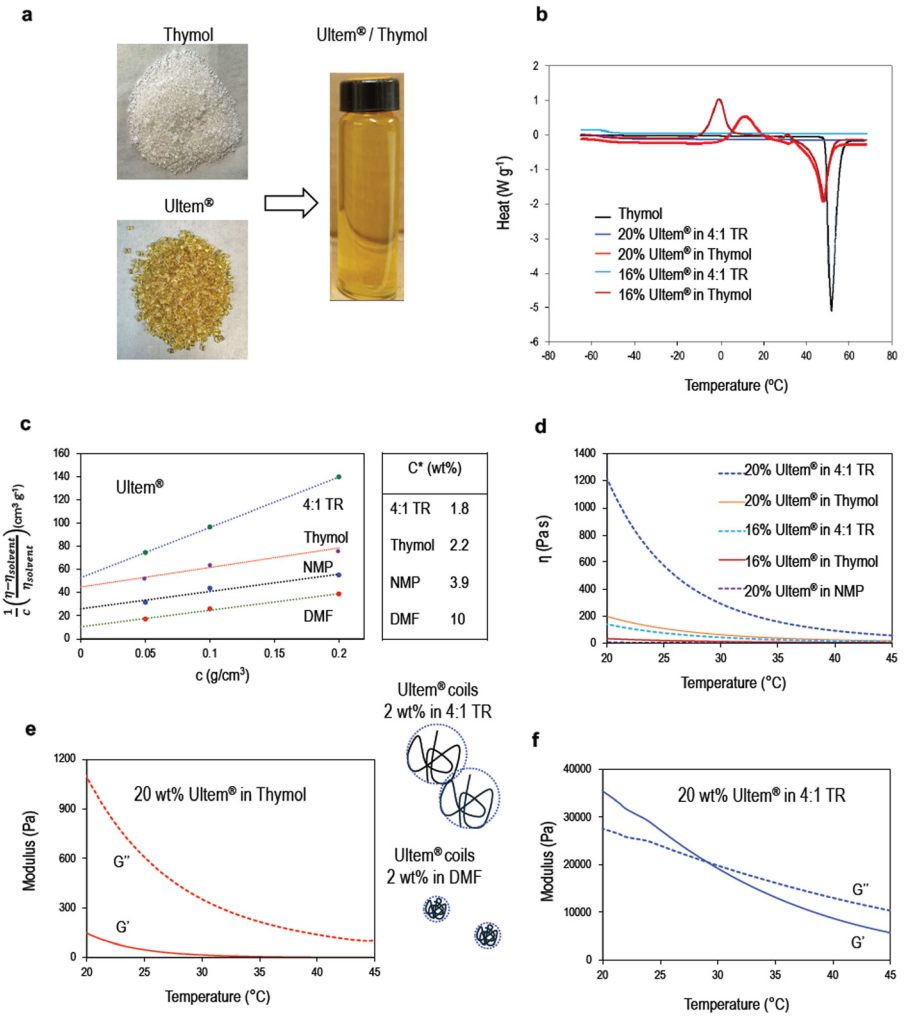

Fig. 2 Physical properties of Ultem® solutions in different solvents. (a) Photograph of thymol, raspberry ketone and a 4 : 1 solution of both. (b) DSC analysis of thymol and Ultem® solutions in thymol and 4 : 1 thymol/raspberry ketone mixtures. (c) Reduced viscosity measured at 25 °C in DMF, NMP and a solution comprising 4 : 1 thymol/raspberry (TR) ketone and at 50 °C in thymol; calculated critical entanglement concentrations C^*. (d) Dynamic viscosity. (e and f) Storage (G') and loss (G'') moduli.

ture is still clearly observed, slightly shifted to 48 °C. Crystallization peaks appear between −10 and 20 °C. While strong hydrogen bonds between thymol and the carbonyl groups of Ultem® enable its solubilization and partially disrupt the packing of thymol molecules, some order remains and is enough to induce crystallization. However, for solutions in 4 : 1 thymol/raspberry ketone, no peak is seen, indicating no crystallization, or melting at least until −70 °C.

The simplest way to understand solubilization is by analyzing the values of Hansen solubility parameters, as reported in Table S4.† The polar and H-bonding contributions to the solubility parameter are closer to that of Ultem® than those of classical organic solvents. The smallest R_a values were calculated for Ultem®/thymol, Ultem®/raspberry ketone and for Ultem® in 4 : 1 mixtures of thymol and raspberry ketone, menthol or camphor. While Hansen solubility parameters are a good starting point to predict potential solvents for a polymer, the theory is based on the principle of "similia similibus solvuntur". The solubility of the systems investigated in this work is much more driven by acceptor-donor hydrogen bonding or Lewis acid–base interactions, which are not considered by the simplified Hansen solubility approach. A further discussion is presented later based on spectroscopy results. An indication of the solvent quality for a specific polymer is given by the critical entanglement concentration, C^*, which indicates how concentrated a solution must be to start promoting the entanglement between polymer coils.[37]

The better the solvent, the expanded is the coil in diluted solutions. More expanded coils start to entangle at lower polymer concentrations. C^* is estimated from values of the inverse of the intrinsic viscosity. From Fig. 1c, we see that the largest C^* values were estimated for NMP and DMF, which are thermodynamically the weakest solvents. Ultem® solutions in thymol and 4 : 1 thymol/raspberry ketone have similar values near 2 wt%. Above this concentration, the coils entangle. In 2 wt% Ultem® solutions in DMF, the polymer coils are compact, minimizing the polymer–solvent interaction. At the concentrations of 13, 16 and 20 wt% the Ultem®, used in dope solutions for hollow fiber fabrication, the polymer coils are highly entangled. The viscosity of the polymer solutions in different solvents is shown in Fig. 1d. The loss and storage moduli of dope solutions in different temperatures and solvents are shown in Fig. 1e, f and Fig. S9.† The storage modulus reflects the elasticity of the solution and gel-like behavior, which is high for 20 wt% Ultem® solutions in a 4 : 1 thymol/raspberry ketone mixture. In contrast, solutions in NMP with the same polymer concentration have low viscosity and liquid-like characteristics. The rheology of the dope solution is a key parameter for hollow fiber spinning.

Spectroscopic analysis of Ultem® and solvent interactions

The interactions between Ultem® and thymol and 4 : 1 thymol/raspberry ketone are understood based on their acceptor/donor character evaluated by spectroscopy, as shown in Fig. 3. The ^{1}H and ^{13}C NMR spectra of Ultem® are shown in Fig. S10 and S11† and those of their 20 wt% solutions in thymol and thymol/raspberry ketone are seen in Fig. 3 and Fig. S12–S21,† including 2D ^{1}H NMR NOESY spectra. As discussed before, the hydroxyl groups of both thymol and raspberry ketone are hydrogen bond donors, while carbonyl groups are hydrogen bond acceptors (interactions depicted in Fig. 3b). Shifts in the thymol proton peak of thymol hydroxyl groups in the presence of Ultem® are seen in Fig. 3a and c. Corresponding shifts in the Ultem® carbonyl and ether peaks are observed in Fig. 3d ^{13}C NMR spectra. A slightly smaller shift is seen in thymol/raspberry ketone. In the latter, the carbonyl of raspberry ketone partially competes for interaction with thymol.

^{1}H-^{1}H NOESY analysis of Ultem® in thymol and Ultem® in thymol/raspberry ketone solutions confirms the intra- and intermolecular interactions (Fig. S19–S21†). In 4 : 1 thymol/raspberry ketone, cross peaks evidence the existence of C–H···O hydrogen bonds between thymol (δ = 5.09 ppm) and raspberry ketone (δ = 5.52 ppm) protons in the $CDCl_3$ solution as shown in the extended region of Fig. S21.†

Throughput screening of hollow fiber fabrication conditions

Membrane technology offers a low energy solution for separations in many industry sectors. The core components are flat sheet membranes configured as plate and frame or spiral wound modules and hollow fiber membrane modules. Hollow fibers are highly utilized for hemodialysis, water desalination, bioreactors, gas separation, dehumidifiers, *etc*. They have a gradient porous morphology customized to suit specific applications. The principle of pore formation is based on a non-solvent-induced phase separation (NIPS) method. A dope solution is spun and coagulated in a non-solvent bath. Several factors affect their fabrication. Among them are the polymer dope concentration, solvent composition, spinning temperature, composition of the coagulation bath and bore fluid, spinneret geometry, gap between spinneret and bath, fiber speed and collecting force. The conditions screening and optimization are material- and time-consuming. A high-throughput automated manipulator was designed to facilitate screening steps. The set-up is depicted in Fig. S22.† Initially, 13 wt% Ultem® solutions in pure thymol and in a 4 : 1 molar thymol mixture with DL-menthol, raspberry ketone, and D-camphor were used as dope solutions for fiber fabrication in the automated manipulator. The temperature was fixed at 70 °C to guarantee that all solutions would be thermodynamically stable and compared under similar conditions. Instead of being spun through a spinneret, a needle was coated by sequential immersion in the dope solution and the coagulation bath, which consisted of 100% ethanol. The morphology of the resulting fibers imaged by field emission scanning electron microscopy (FESEM) is shown in Fig. S23.† Hollow fibers prepared using thymol mixtures with menthol and camphor were fully sponge-like, while those with pure thymol or a mixture with raspberry ketone had finger-like structures. The speed of solvent and non-solvent exchange during the pore formation is highly relevant for the morphology. The kinetics of solvent exchange depends on the viscosity of the dope solution and on the thermodynamic interaction between the solvent

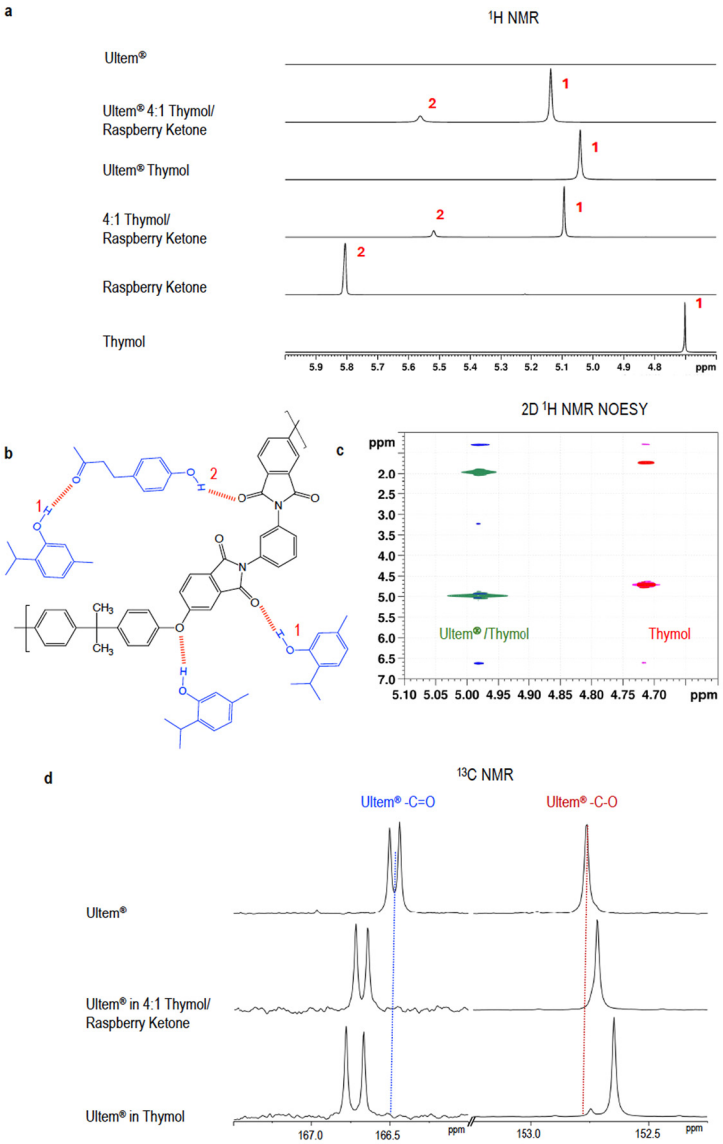

Fig. 3 NMR spectroscopy analysis of Ultem® solutions. (a) ^{1}H NMR spectra of different solutions and individual components. (b) Hydrogen bond structures between Ultem®, thymol and raspberry ketone. (c) 2D ^{1}H NMR NOESY overlap spectra of thymol and Ultem®/thymol. (d) ^{13}C NMR spectra of Ultem® and its solutions in thymol and in 4 : 1 thymol/raspberry ketone.

and non-solvent. Ethanol was used as the non-solvent in the coagulation bath. The ethanol Hansen solubility parameters are δ_d = 15.80, δ_p = 8.80, δ_h = 19.40. D-Camphor (δ_h = 4.7) is the solvent with the lowest similarity to ethanol, at least in terms of δ_h value expecting a lower driving force for exchange. More relevant are the differences in viscosity at the temperatures of fiber formation. High viscosities promote a slow exchange and a sponge-like structure. Low viscosity in contrast facilitates a rapid intrusion of the non-solvent and the consequent finger-like structures (as in the case of thymol δ_h = 10.8).

Large-scale hollow fiber fabrication by dry–jet wet spinning

When the industrial fabrication is targeted, processes close to room temperature are preferred. Therefore, Ultem® dope solutions in pure thymol or thymol/raspberry ketone were selected for hollow fiber fabrication upscale in a pilot continuous dry–jet wet machine depicted in Fig. S24.† In this case, unlike in the automated manipulator, the dope solution is extruded through a spinneret into the coagulation bath and a bore fluid is injected into the lumen of the incipient fiber. The solvent–non-solvent exchange and phase separation process simultaneously start from the lumen and the shell side of the fiber. Ethanol and a mixture of 50% ethanol/water were used as the non-solvents in the coagulation bath. The coagulation baths were re-used in the entire study. The conditions for spinning hollow fibers are detailed in Table S5.†

The FESEM images (cross-sectional and surface images of the lumen and shell side) of the fibers are shown in Fig. 4a

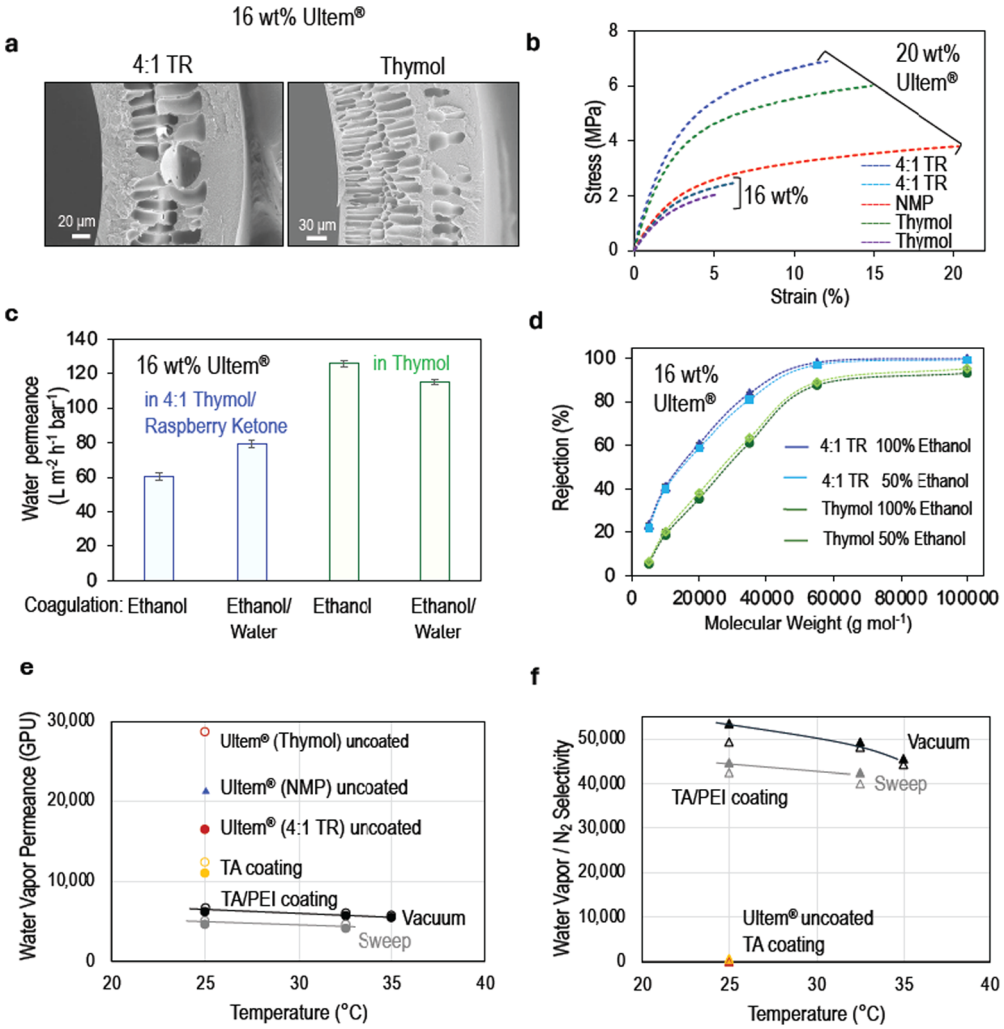

Fig. 4 Characterization of hollow fibers. (a) FESEM cross-sectional images of hollow fibers fabricated from 16 wt% Ultem® solutions in thymol and in 4 : 1 thymol/raspberry ketone coagulated in ethanol. (b) Stress–strain curves of hollow fibers prepared from different dope solutions. (c) Water permeance of hollow fibers prepared from 16 wt% Ultem® solutions in thymol and in 4 : 1 thymol/raspberry ketone coagulated in ethanol and in 1 : 1 ethanol/water. (d) Rejection of polyethylene glycol with different molecular weights. (e) Water vapor permeance and (f) water vapor/N_2 selectivity of uncoated hollow fibers prepared from solutions in different solvents before and after coating with tannic acid (TA) and TA/hyperbranched polyethyleneimine (PEI) as a function of temperature. Experiments were performed under vacuum and sweep gas.

and Fig. S25, S26.† The 16 wt% Ultem® dope solution with 4 : 1 thymol/raspberry ketone has a viscosity of 11.0 Pa s while with pure thymol, the viscosity is 4.0 Pa s at 45 °C. Symmetric finger-like cavities are formed. When the polymer concentration is increased to 20 wt%, the viscosity rises to 56 and 20 Pa s, respectively, leading to slower phase separation and higher resistance for intrusion of the non-solvent. A sponge-like structure is then favored.

Fig. 4b and Fig. S27† showcase the mechanical properties of the hollow fibers prepared from dope solutions in thymol, 4 : 1 thymol/raspberry ketone and *N*,*N*-methyl pyrrolidone. The fibers produced from solutions in the newly proposed green solvents are mechanically stronger than those prepared in NMP and can withstand higher stress. The viscosity and the loss modulus of dope solutions in NMP are lower (see Fig. 2d and Fig. S9†). The Young's modulus, toughness, tensile strength, and elongation at break values are similar for fibers prepared from dope solutions in thymol and in 4 : 1 thymol/raspberry ketone at concentrations 16 wt% and 20 wt% Ultem®. Fig. S28† confirms that thymol is not present in the fibers after fabrication.

Fig. 4c and d show the pure water permeance and molecular weight cut-off estimation curves for hollow fibers fabricated from 16 wt% Ultem® dope solutions in thymol and 4 : 1 thymol/raspberry ketone. The latter have permeances of 60.5 and 79.3 L m^{-2} h^{-1} bar^{-1}, as the bore fluid shifted from 100% ethanol to 1 : 1 ethanol/water. The permeances were higher for membranes produced from thymol, with permeance values of 126 and 112 L m^{-2} h^{-1} bar^{-1} when coagulated in 100% ethanol and 1 : 1 ethanol/water, respectively.

Coating and characterization of hollow fibers for air dehumidification

We recently prepared Ultem® hollow fibers from dope solutions in NMP.[38–40] We have explored diethyleneglycol as a pore-forming agent, along with different spinning parameters, to obtain various supports which were successfully used for gas dehydration applications with specialized coatings. These fibers have a porosity of around 72.3% with a water vapor permeance of 20 353 ± 833 GPU and a selectivity of 9.0 ± 0.9 for water vapor over nitrogen.[38] We have coated the fibers with a green polyphenol (tannic acid) that has a high-water vapor transport rate, ranging from 4900 to 13 000 GPU. This coating has the potential to be used for air dehydration applications in areas such as air conditioning, food packaging, space applications, and flue/syngas dehydration. The coated fibers were then treated with hyperbranched polyethyleneimine (PEI), which increased the water/N_2 selectivity from 356 to 47 300 based on coating time.

The hollow fibers prepared in this work with greener solvents were coated with the same procedure, and the performance is plotted in Fig. 4e. The uncoated spun fibers exhibited a water vapor transport rate of 16 453 GPU and 28 633 GPU when using 16 wt% Ultem® dope solutions in 4 : 1 thymol/raspberry ketone and in pure thymol, respectively. A 41% increase in water vapor flux was achieved compared to fibers prepared from solutions in NMP with similar selectivity for water vapor over nitrogen. Fig. 4e and f show the membrane performance for polyphenol coating at different temperatures and modes of operation (applying vacuum or sweep gas on the permeate side). The water vapor permeance rate between 4000 and 12 500 GPU (Table S6†) similar to results obtained with fibers prepared from dope solutions in NMP and coated with polyphenol. The membranes had a water/N_2 selectivity up to 49 000 after coating, proving to be a greener replacement for traditional supports as well as for solvents in membrane fabrication.

Conclusions

Thymol is proposed as a green solvent for polyetherimide leading to liquid homogeneous solutions, which could be successfully applied for the fabrication of hollow fibers for air dehumidification. The peculiar liquid solution constituted by a high molecular polymer and a natural terpene, both solid as single compounds at room temperature, have analogy to what has been previously observed for pairs of small molecules. Hence, we classify it as a "deep eutectic polymer system" (DEPS). The solutions were fully characterized by NMR spectroscopy, thermal analysis and rheological methods. The evidence confirmed that hydrogen bonding is the major factor for solubilization. Mixtures of thymol and other natural products were also successfully evaluated as solvents. The quality of the proposed green solvents is thermodynamically superior to classical organic solvents like DMF or NMP.

The solutions were applied for hollow fiber spinning which were tested for ultrafiltration. When coated with polyphenols, the fibers were tested for water vapor transport for dehumidification. The results provide solutions for membrane production under increasingly stricter environmental rules for the use of chemicals. Long-term separation applications for membranes include biorefineries and the pharmaceutical and petrochemical industries.

Experimental

Materials

Polyetherimide, Ultem® 1000, was purchased from SABIC (USA). Thymol, DL-menthol, raspberry ketone (4-(4-hydroxyphenyl)-2-butanone), and D-camphor were procured from Sigma Aldrich (UK). The reagents for the hollow fiber coating, tannic acid, sodium periodate ($NaIO_4$) and hyperbranched polyethyleneimine (PEI) of molecular weight 25 000 g mol^{-1} were purchased from Sigma Aldrich (UK). Other solvents like *N*-methyl-2-pyrrolidone (NMP), *N*,*N*-dimethylformamide (DMF) and ethanol were obtained from Fisher Scientific (UK). All solvents and reagents were used as received.

Preparation and characterization of Ultem® solutions

Thymol, a hydrophobic monoterpene, was used as the main solvent component. Other hydrophobic compounds with varied melting points included DL-menthol (another monoterpene) and aroma compounds such as raspberry ketone and D-camphor. The molar compositions of thymol to the secondary component were varied as 1 : 4, 1 : 1 and 4 : 1. 13 wt%, 16 wt% and 20 wt% Ultem® 1000 was dissolved in the different solvent mixtures and in pure thymol by stirring overnight at 250 rpm and at 85 °C.

Calorimetric characterization

The thermal transitions of the selected mixtures and thymol-based dope solutions were measured using a differential scanning calorimeter, DSC Q-200 (TA Instruments, USA). The samples were initially weighed and placed in T_{zero} hermetic pans. During the analysis, the thermal history of the sample was removed by initially heating the samples from 25 °C to 100 °C and maintaining them isothermally at 100 °C for 1 min. Subsequently, the samples were cooled at a 10 °C min^{-1} rate to −70 °C and maintained isothermally at −70 °C for 5 min before being heated to 80 °C at a 10 °C min^{-1} rate. Following this, the samples were cooled to 25 °C.

Rheological characterization

The rheological properties of various dope solutions were investigated on an AR-2000ex rheometer (TA Instruments Ltd, New Castle, USA). The dynamic viscosity of the dope solutions was measured over a temperature range of 20 °C–45 °C. The maximum temperature of measurement corresponds to the temperature at which the hollow fibers were fabricated by the dry–jet wet spinning process. The viscoelastic behavior of dope

solutions was studied with oscillatory measurements, in which a sinusoidal strain is applied. An amplitude sweep was used to define the linear viscoelastic range of samples without the risk of exceeding the strain value and destroying the structure.[41] The amplitude sweep was measured from the strain 0.01 to 1000% with an angular frequency of 10 rad s^{-1}. The linear viscoelastic range was identified between 0.01 and 100%. The storage modulus G' and the loss modulus G'' of the dope solutions were plotted in the temperature range of 20 °C–45 °C.

Nuclear magnetic resonance (NMR)

To investigate the intermolecular hydrogen bonding between the components, Ultem®, the solvent mixtures and their individual components (30–40 mg) were dissolved in $CDCl_3$ (600 μL), and the ^1H and ^{13}C NMR spectra were acquired at 25 °C on a Bruker SB Liquid 500 MHz NMR spectrometer (respectively, operating at 500.1 and 125.7 MHz). The relaxation time between the repetitions ($d1$) was set to 4 s, and the number of scans (NS) of 64 and 256 was applied in the ^1H and ^{13}C NMR spectrum acquisition, respectively. Additionally, ^1H–^1H NOESY and ^1H–^{13}C ROESY 2D experiments were performed on the same equipment. Spectra were calibrated using the residual $CHCl_3$ proton signal at 7.28 ppm and the carbon signal at 77.16 ppm and further analysed using the Bruker TopSpin 4.3.0 software.

The hydrogen-bond-accepting abilities of Ultem® and solvent components were further quantified using ^{31}P NMR spectroscopy with triethylphosphine oxide (TEPO) as a commercially available probe. The compounds and the probe were freeze-dried, mixed (compound : probe molar ratio = 3 : 1) and dissolved in $CDCl_3$ (600 μL). ^{31}P NMR spectra (NS = 16) were collected at 25 °C on a Bruker Avance III 600 MHz NMR spectrometer operating at 242.9 MHz.

Fabrication of hollow fibers by an automated manipulator unit

To enable a quick screening of optimal conditions for rapid preparation of hollow fibers, an automated manipulator unit was designed and built using an advanced 3D printer (see Fig. S22†). The functioning of the unit is based on the recently reported work that showcases the rapid fabrication of short-length hollow fibers.[42] In brief, the manipulator unit consists of a platform with 25 glass vial holders. From the top, an empty syringe with a needle is transfixed to the syringe holder that can move in the x, y, and z axes. The manipulator is connected to software that can set an algorithm for the speed and direction of the movements of the syringe in all the three axes. Particularly, the operating parameters like the speed of the syringe to enter the glass vial filled with the dope solution, the dwelling time, and the uptake speed of the syringe were optimized. Subsequently, the needle was detached and placed in a glass vial for precipitation up to 24 h with 2 intervals of replacement of the coagulation bath to ensure the complete removal of the natural green solvent(s) from the hollow fibers. The solvents have characteristic odors identified even in low amounts.

The dope solutions were prepared by dissolving Ultem® in the different solvents. Various screening parameters such as concentration of Ultem®, type of precipitation bath, temperature and duration of the experiments were considered.

Hollow fibers prepared by a dry–jet wet spinning unit

The Ultem®-in-DES and Ultem®-in-thymol based hollow fibers were prepared by nonsolvent-induced phase separation using a dry jet wet-spinning process.[38] Fig. S24† depicts the schematic representation of the dry–jet wet spinning unit. Detailed information about the spinning conditions is presented in Table S5.†

The fibers were fabricated using the free fall method with 100% ethanol as the bore fluid. The prepared solutions were transferred to a feed tank and left untouched for 24 h to remove any air bubbles. The feed tank was wrapped with heating coils and connected to a temperature controller. After 24 h of residence time, spinning was initiated after applying an upstream pressure of 1.5 to 3.3 bar, based on the viscosity of the dope solution. After spinning, depending on the coagulation bath used, the membranes were conditioned either in ethanol or in a mixture of 50% ethanol and 50% water for two days to facilitate solvent exchange. This also ensures the complete removal of the natural green solvent(s) and any remaining odor from the hollow fibers. Subsequently the hollow fibers were dried for further use.

Coating of hollow fibers for air dehumidification

The coating and crosslinking of the selected hollow fibers for enhanced water vapor removal were undertaken by a dip-coating method using tannic acid, sodium periodate ($NaIO_4$) and hyperbranched polyethyleneimine (PEI), as recently reported by us.[38] The experimental method used to assess the performance of the composite membranes involved a combination of water vapor and nitrogen gas. The setup involves using a sweep gas or vacuum to maintain a consistent driving force. Humidity and temperature sensors were utilized to take precise readings on both the feed and permeate sides.

Characterization of hollow fibers

The membrane morphology and the cross-sectional structure of the hollow fibers were analyzed using a ZEISS Merlin Gemini and FEI Nova Nano field-emission scanning electron microscope. To prepare the samples for cross-sectional characterization, the membrane samples were freeze-dried and fractured in liquid nitrogen. The subsequent sputter-deposition was carried out using 5 nm of Ir using a K575X Emitech equipment.

To determine the mechanical stability of the hollow fibers, the strain *vs.* stress measurements of the membranes were performed on a Discovery DMA850 instrument (TA instruments, USA). The stress ramp was set at a rate of 1.5 N min^{-1} from 0.05 N to 18.00 N. Subsequently, the Young's modulus (the slope of the linear elastic behavior), fracture strain (the maximum value of strain just before the sample broke), tensile strength (the maximum value of stress at which the sample

broke), and toughness (the area calculated under the strain *vs.* stress curve) were evaluated from the strain *vs.* stress curve.[43] All the measurements were carried out in triplicate and the average value was reported.

For measuring liquid water permeance, a feed solution of pure water was circulated into the shell side, while the lumen side was used to collect the permeate. The pure water permeance PWP (L m^{-2} bar^{-1} h^{-1}) was determined by circulating water into the module at a flow rate of 0.13 L min^{-1} under a pressure of 1 bar. The PWP value was then calculated using the following equation:

$$PWP = \frac{Q}{\Delta P X A_m} \quad (1)$$

where Q is the water permeation volumetric flow rate (L h^{-1}), A_m is the effective area (m^2), and ΔP is the transmembrane pressure (bar).

Experimental analysis was conducted to evaluate the rejection profile of PEI hollow fibers. The analysis was carried out by performing solute rejection experiments with 200 ppm of neutral organic solutes, including PEG and PEO with different molecular weights, at 1 bar. Prior to the collection of feed and permeate, the system was stabilized for an hour. The feed and permeate were collected three times at consecutive time intervals of 0.5 h, and the concentrations of feed and permeate were measured by gel permeation chromatography using the 1260 Infinity GPC/SEC equipment from Agilent Technologies (USA). The solute rejection R_T (%) was calculated using the following equation:

$$R_T(\%) = 1 - \left(\frac{c_p}{c_f}\right) \quad (2)$$

where c_p and c_f are the solute concentrations in the permeate and feed solutions, respectively.

The water vapor flow rate through the membrane was estimated using eqn (3):

$$Q_{vapor} = Q_{N_2} \times \gamma_{H_2O} \times \left(\frac{V_m}{M_{w,H_2O}}\right) \quad (3)$$

where Q_{N_2} (cm^3 s^{-1}) is the nitrogen flow rate at the permeate side, γ_{H_2O} (g m^{-3}) is the absolute humidity, V_m (L mol^{-1}) is the volume of 1 mol of penetrant at standard temperature and pressure, and M_{w,H_2O}, (g mol^{-1}) is the molecular weight of water.

The water vapor permeance was estimated using eqn (4):

$$\text{Permeance} = \frac{Q_{vapor}}{A \times \Delta P} \quad (4)$$

where A (cm^2) is the area of the membrane, and ΔP (cmHg or kPa) is the partial pressure difference across the membrane. The permeance is expressed in the Gas Permeation Unit (GPU), where 1 GPU = 10^{-6} cm^3 (STP) cm^{-2} s^{-1} $cmHg^{-1}$ = 7.6 × 10^{-9} m^3 (STP) m^{-2} s^{-1} kPa^{-1}.

The selectivity of the membrane for water vapor over nitrogen was calculated using eqn (5):

$$\text{Selectivity} = \frac{\text{Water vapor permeance}}{\text{Nitrogen permeance}} \quad (5)$$

Author contributions

U.T.S, L.U. and S.N. conceived the project and designed the experiments. U.T.S. synthesized and characterized the green solvents and dope solutions. L.L. and A-H.E. performed the N. M.R. experiments. A.V. developed the in-house manipulator unit and with U.T.S., the hollow fibers were rapidly fabricated. L.U. and U.T.S. fabricated and characterized the hollow fibers produced by the dry–jet wet spinning unit. L.U. modified the hollow fibers for air dehumidification studies. U.T.S., L.U. and S.N. wrote the manuscript.

Data availability

The data supporting this article have been included as part of the ESI.†

Conflicts of interest

There are no conflicts to declare.

Acknowledgements

This work was sponsored by King Abdullah University of Science and Technology (KAUST), OFP 2023 grant URF/1/5614-01-01 “Sustainable membrane fabrication for organic solvent nanofiltration”. Fig. S22 and S24† were produced by Ana Bigio, scientific illustrator.

References

1 F. Borchert, A. Beronius and M. Ågerstrand, *Environ. Sci. Eur.*, 2022, **34**, 83.
2 E. C. A. (ECHA), *N*,*N*-Dimethylformamide restricted from December 2023, **https://echa.europa.eu/view-article/-/journal_content/title/9109026-58**).
3 A. Jordan, C. G. Hall, L. R. Thorp and H. F. Sneddon, *Chem. Rev.*, 2022, **122**, 6749–6794.
4 D. Zou, S. P. Nunes, I. F. Vankelecom, A. Figoli and Y. M. Lee, *Green Chem.*, 2021, **23**, 9815–9843.
5 United States Environment Protection Agency (EPA), Chemicals under the Toxic Substances Control Act (TSCA), **https://www.epa.gov/chemicals-under-tsca**, (accessed 23/11/2023).
6 United States Occupational Safety and Health Administration (OSHA) agency, Transitioning to Safer Chemicals: A Toolkit for Employers and Workers, **https://www.osha.gov/chemical-hazards**, (accessed 23/11/2023).
7 E. Durand, P. Villeneuve, C. Bourlieu-Lacanal and F. Carrière, in *Advances in Botanical Research*, Elsevier, 2021, vol. 97, pp. 133–158.

8 R. Craveiro, F. Mano, A. Paiva and A. R. C. Duarte, *Deep Eutectic Solvents: Synthesis, Properties, and Applications*, 2019, pp. 95–110.
9 C. He, I. Gállego, B. Laughlin, M. A. Grover and N. V. Hud, *Nat. Chem.*, 2017, **9**, 318–324.
10 Y. Dai, G.-J. Witkamp, R. Verpoorte and Y. H. Choi, *Anal. Chem.*, 2013, **85**, 6272–6278.
11 A. P. Abbott, G. Capper, D. L. Davies, R. K. Rasheed and V. Tambyrajah, *Chem. Commun.*, 2003, 70–71.
12 Y. H. Choi, J. van Spronsen, Y. Dai, M. Verberne, F. Hollmann, I. W. Arends, G.-J. Witkamp and R. Verpoorte, *Plant Physiol.*, 2011, **156**, 1701–1705.
13 Q. Zhang, K. D. O. Vigier, S. Royer and F. Jérôme, *Chem. Soc. Rev.*, 2012, **41**, 7108–7146.
14 J. Afonso, A. Mezzetta, I. Marrucho and L. Guazzelli, *Green Chem.*, 2023, **25**, 59–105.
15 E. L. Smith, A. P. Abbott and K. S. Ryder, *Chem. Rev.*, 2014, **114**, 11060–11082.
16 P. Willberg-Keyriläinen, J. Hiltunen and J. Ropponen, *Cellulose*, 2018, **25**, 195–204.
17 J. L. de Lacalle, A. Gallastegui, J. L. Olmedo-Martínez, M. Moya, N. Lopez-Larrea, M. L. Picchio and D. Mecerreyes, *ACS Macro Lett.*, 2023, **12**, 125–132.
18 C. Mukesh, R. Gupta, D. N. Srivastava, S. K. Nataraj and K. Prasad, *RSC Adv.*, 2016, **6**, 28586–28592.
19 J. Wang, S. Zhang, Z. Ma and L. Yan, *Green Chem. Eng.*, 2021, **2**, 359–367.
20 L. Ren'ai, K. Zhang, G. Chen, B. Su, J. Tian, M. He and F. Lu, *Chem. Commun.*, 2018, **54**, 2304–2307.
21 X. Li, J. Liu, Q. Guo, X. Zhang and M. Tian, *Small*, 2022, **18**, 2201012.
22 A. R. S. Santha Kumar and N. K. Singha, *J. Polym. Sci., Part A: Polym. Chem.*, 2019, **57**, 2281–2286.
23 F. Russo, M. Tiecco, F. Galiano, R. Mancuso, B. Gabriele and A. Figoli, *J. Membr. Sci.*, 2022, **649**, 120387.
24 R. Castro-Muñoz, F. Galiano, A. Figoli and G. Boczkaj, *J. Environ. Chem. Eng.*, 2022, **10**, 106414.
25 N. Ismail, J. Pan, M. Rahmati, Q. Wang, D. Bouyer, M. Khayet, Z. Cui and N. Tavajohi, *J. Membr. Sci.*, 2022, **646**, 120238.
26 A. Y. Gebreyohannes, S. L. Aristizabal, L. Silva, E. A. Qasem, S. Chisca, L. Upadhyaya, D. Althobaiti, J. A. Coutinho and S. P. Nunes, *Green Chem.*, 2023, **25**, 4769–4780.
27 J. Cao and E. Su, *J. Cleaner Prod.*, 2021, **314**, 127965.
28 W. Chen, X. Li, L. Chen, G. Zhou, Q. Lu, Y. Huang, Y. Chao and W. Zhu, *Chem. Eng. J.*, 2021, **420**, 127648.
29 C. Florindo, L. C. Branco and I. M. Marrucho, *ChemSusChem*, 2019, **12**, 1549–1559.
30 S. Mondal, U. T. Syed, C. Gil, L. Hilliou, A. F. Duque, M. A. Reis and C. Brazinha, *Green Chem.*, 2023, **25**, 1137–1149.
31 U. T. Syed, I. C. Leonardo, G. Mendoza, F. B. Gaspar, E. Gámez, R. M. Huertas, M. T. Crespo, M. Arruebo, J. G. Crespo and V. Sebastian, *Sep. Purif. Technol.*, 2022, **285**, 120319.
32 D. J. Van Osch, C. H. Dietz, S. E. Warrag and M. C. Kroon, *ACS Sustainable Chem. Eng.*, 2020, **8**, 10591–10612.
33 S. Mondal, U. Syed, E. Pinto, I. Leonardo, P. Romero, F. Gaspar, M. B. Crespo, V. Sebastian, J. Crespo and C. Brazinha, *J. Cleaner Prod.*, 2024, **444**, 141167.
34 S. Xiang, G. Yu, Y. Liang and L. Wu, *J. Mol. Struct.*, 2006, **789**, 43–51.
35 M. Milic, K. Targos, M. Tellez Chavez, M. A. Thompson, J. J. Jennings and A. K. Franz, *J. Org. Chem.*, 2021, **86**, 6031–6043.
36 J. J. Jennings, M. Milic, K. Targos and A. K. Franz, *Eur. J. Med. Chem.*, 2020, **207**, 112693.
37 D. Kim, H. Vovusha, U. Schwingenschlögl and S. P. Nunes, *J. Membr. Sci.*, 2017, **539**, 161–171.
38 L. Upadhyaya, A. Y. Gebreyohannes, M. W. Shahzad, U. T. Syed, S. L. Aristizábal, R. Gorecki and S. P. Nunes, *J. Membr. Sci.*, 2023, 122215, DOI: **10.1016/j.memsci.2023.122215**.
39 A. Y. Gebreyohannes, L. Upadhyaya, L. P. Silva, G. Falca, P. J. Carvalho and S. P. Nunes, *ACS Sustainable Chem. Eng.*, 2020, **8**, 17763–17771.
40 L. Upadhyaya, A. Y. Gebreyohannes, F. H. Akhtar, G. Falca, V. Musteata, D. K. Mahalingam, R. Almansoury, K. C. Ng and S. P. Nunes, *J. Membr. Sci.*, 2020, **614**, 118450.
41 R. Esposito, V. Musteata, S. Chisca and S. P. Nunes, *ACS Appl. Polym. Mater.*, 2021, **3**, 6045–6055.
42 T. Anokhina, A. Raeva, S. Makaev, I. Borisov, V. Vasilevsky and A. Volkov, *Membranes*, 2021, **11**, 396.
43 M. Ramírez-Martínez, S. L. Aristizábal, G. Szekely and S. P. Nunes, *Green Chem.*, 2023, **25**, 966–977.